Dalton Transactions

PAPER

View Article Online
View Journal | View Issue

Cite this: *Dalton Trans.*, 2016, **45**, 17409

In search of molecules displaying ferromagnetic exchange: multiple-decker Ni_{12} and Ni_{16} complexes from the use of pyridine-2-amidoxime†

Constantinos G. Efthymiou,[a,b] Luís Cunha-Silva,[c] Spyros P. Perlepes,[b] Euan K. Brechin,[d] Ross Inglis,*[d] Marco Evangelisti*[e] and Constantina Papatriantafyllopoulou*[a]

Received 8th September 2016,
Accepted 26th September 2016

DOI: 10.1039/c6dt03511f

www.rsc.org/dalton

The use of pyridine-2-amidoxime ($pyaoxH_2$) in Ni chemistry has provided access to a dodecanuclear complex and a hexadecanuclear Ni cluster, namely $[Ni_{12}(pyaox)_6(pyaoxH)_6(MeOH)_2Cl_2]Cl_4{\cdot}5MeOH$ (**1**·5MeOH) and $[Ni_{16}(pyaox)_8(pyaoxH)_8(MeOH)_4](SO_4)_4{\cdot}10H_2O{\cdot}26MeOH$ (**2**·$10H_2O$·26MeOH). Complex **1**·5MeOH was isolated by the reaction of $NiCl_2{\cdot}6H_2O$, $pyaoxH_2$ and NaOMe in a 1 : 1 : 2 molar ratio in MeOH in 60% yield. Treatment of $NiSO_4{\cdot}6H_2O$ with $pyaoxH_2$ and NEt_3 in a 1 : 1 : 2 molar ratio in MeOH afforded **2**·$10H_2O$·26MeOH in good yield (65%). The two compounds display a multi-decker configuration based on stacked Ni_4 layers, $\{Ni_4(pyaox)_2(pyaoxH)_2\}^{2+}{}_x$ (x = 3, **1**·5MeOH; x = 4, **2**·$10H_2O$·26MeOH); each deck consists of two square planar and two octahedral Ni^{II} centres. The number of decks observed in **1**·5MeOH and **2**·$10H_2O$·26MeOH depends on the nature of the inorganic anion that is present in the reaction system, which provides elements of synthetic control towards new high nuclearity Ni^{II} species. **2**·$10H_2O$·26MeOH is the first structurally characterized complex of any metal displaying a quadruple-decker configuration, being also the highest nuclearity metal cluster bearing $pyaoxH_2$ and the highest nuclearity Ni^{II} cluster with any type of 2-pyridyl oxime. Each cluster cation displays ferromagnetic exchange between the octahedral Ni^{II} ions resulting in a spin ground state of S = 6 for **1** and S = 8 for **2**. Magnetothermal studies have been performed and discussed for both clusters.

Introduction

It has been over 20 years since the discovery that the discrete $[Mn_8^{III}Mn_4^{IV}O_{12}(O_2CMe)_{16}(H_2O)_4]$ molecule could possess an energy barrier to its spin vector reversal that was large enough to observe magnetic hysteresis, the classical property of a magnet.[1] This discovery constituted the commencement of a new era in transition metal cluster chemistry, sparking off intense interest in the synthesis and characterization of new coordination compounds that could behave like magnets at very low temperatures in the absence of an applied magnetic field. Such species are now known as single-molecule magnets (SMMs)[2] with their properties originating from intrinsic structural and electronic characteristics of their metal cores. The potential applications of SMMs range from high-density information storage, molecular spintronics, to qubits for quantum computation.[3–5] Furthermore, several other quantum mechanical phenomena have been identified in SMMs, such as spin-phonon coupling,[6] spin state entanglement,[5] spin parity effects,[7] both thermally assisted and pure quantum tunneling of the magnetization (QTM),[8] and quantum phase interference.[7b,9]

Clusters containing Mn^{III} ions have proven to be the most fruitful source of SMMs to date. This is not surprising considering that: (1) the first and most well-known SMM comes from Mn cluster chemistry, a fact that activated intense research in this area, and (2) the d^4 Mn^{III} ion displays significant anisotropy, an inherent requirement for the generation of new SMMs.[2] However, SMMs are also known for 3d metal ions

[a]*School of Chemistry, National University of Ireland Galway, University Road, Galway, Ireland. E-mail: constantina.papatriantafyllopo@nuigalway.ie; Tel: +353 91 493462*
[b]*Department of Chemistry, University of Patras, 26504 Patras, Greece*
[c]*REQUIMTE-LAQV, Department of Chemistry and Biochemistry, Faculty of Sciences, University of Porto, 4169-007 Porto, Portugal*
[d]*EastCHEM School of Chemistry, The University of Edinburgh, David Brewster Road, EH9 3FJ Edinburgh, UK. E-mail: r.inglis@ed.ac.uk; Tel: +44 (0)11 650470*
[e]*Instituto de Ciencia de Materiales de Aragón (ICMA), CSIC-Universidad de Zaragoza, Departamento de Fisica de la Materia Condensada, 50009 Zaragoza, Spain. E-mail: evange@unizar.es; Tel: +34-876-55-3342*

†Electronic supplementary information (ESI) available: Tables with bond distances and angles, hydrogen bonding details, magnetism and heat capacity plots for **2**·$10H_2O$·26MeOH. CCDC 678537 and 1502969. For ESI and crystallographic data in CIF or other electronic format see DOI: 10.1039/c6dt03511f

other than Mn, *e.g.* V^{III}, Fe^{II}, Fe^{III}, Ni^{II}, lanthanide ions, actinide ions, and combinations of 3d with 4d, 5d or 4f paramagnetic metal ions.[2,10] Among them, Ni^{II} has shown much promise in the synthesis of both SMMs[11] and spin phonon traps,[12] due to its significant single-ion anisotropy and its paramagnetic nature when confined within a highly symmetric cage.

The isolation of new SMMs remains a hot research field, not only for a better understanding of the phenomenon but also for bringing these species closer to technological applications. In fact, the chances of identifying novel types of coordination clusters with improved or new magnetic properties will be increased by the development of new reaction systems with suitable organic ligands or combinations of organic and inorganic ligands. The organic ligand often dictates the cluster symmetry, metal topology and the number of metal ions that are present, which in turn affects the nature of the magnetic exchange interactions and the intermolecular interactions between the polynuclear molecules in the crystal. One fertile approach towards the synthesis of new polynuclear metal complexes with interesting magnetic properties is the use of oxime ligands, since oximates are good bridging groups fostering formation of coordination clusters.[13] We and others have been investigating a number of oxime-based ligands, and one broad family of the latter has been the 2-pyridyl oximes (Scheme 1).[14] The anions of 2-pyridyl oximes are versatile ligands for a variety of research objectives; the activation of 2-pyridyl oximes by 3d-metal centres towards further reaction is also becoming an exciting area of research.[15] Such ligands have been key "players" in several areas of single-molecule and single-chain magnetism.[16]

Restricting further discussion to nickel, our groups have been engaged in the use of 2-pyridyl oximate ligands for Ni^{II} cluster synthesis for many years. The first step of this approach included the synthesis and characterization of complexes of pao^-,[17] $mpko^-$ [18] and $ppko^-$,[17e,18c,d,19] *i.e.*, complexes bearing anionic ligands in which R contains no additional donor site. In a second step, we have been studying Ni^{II} complexes with anionic ligands in which R contains a donor site, *i.e.*, clusters of $(py)pko^-$ [17a,20] and $pyaoxH^-/pyaox^{2-}$.[21] In particular, the ligand $pyaoxH_2$ (pyridine-2-amidoxime; IUPAC name: *N*-hydroxy-pyridine-2-carboxamidine) belongs to the class of amidoximes. Although the versatile chemistry of conventional oximes has been extensively studied over the years in both the organic chemistry and coordination chemistry literature, amidoximes, $RC(NH_2)$ = NOH, have so far received substantially less attention.[22] The presence of the amino functionality is expected – due to its coordination capability, potential for deprotonation and hydrogen bonding effects – to alter the coordination behaviour of this ligand (and hence the identity of the resultant Ni^{II} complexes) in comparison with that of the pao^-, $mpko^-$, $ppko^-$, $(py)pko^-$, *etc.*, ligands.

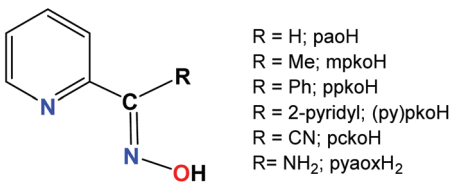

R = H; paoH
R = Me; mpkoH
R = Ph; ppkoH
R = 2-pyridyl; (py)pkoH
R = CN; pckoH
R= NH_2; $pyaoxH_2$

Scheme 1 General structural formula and abbreviations of the 2-pyridyl oximes discussed in the text.

In 2008, our groups employed $pyaoxH_2$ in Ni cluster chemistry and proved that it can be a fruitful method for the synthesis of high nuclearity species.[21] Nevertheless, the use of $pyaoxH_2$ for the synthesis of polynuclear Ni compounds remains limited.[21,23–25] In particular, so far there have been reports of only salts of the cations $[Ni_4(pyaox)_2(pyaoxH)_2L_4]^{2+}$ (L = imidazole, 1-methylimidazole, pyridine, 3-methylpyridine, 4-methylpyridine),[23,24] $[Ni_8(pyaox)_4(pyaoxH)_4L'_4]$ (L′ = H_2O, imidazole),[23,24] $[Ni_{12}(pyaox)_6(pyaoxH)_6(H_2O)_2(N_3)_2]^{4+}$ and $[Ni_{12}(pyaox)_6(pyaoxH)_6(H_2O)_2]^{6+}$.[21,23,24] The cations have single-(Ni_4), double-(Ni_8) and triple-decker (Ni_{12}) structures, where each deck is composed of the same tetranuclear cationic unit $\{Ni_4(pyaox)_2(pyaoxH)_2\}^{2+}$ (proved to be present in solution by ESI-MS spectrometry[23,24]) and features two square planar and two octahedral Ni^{II} centres.

In this work, we expand the above mentioned family of multiple-decker Ni clusters by reporting the syntheses, crystal structures and magnetic and heat capacity properties of two such species, namely $[Ni_{12}(pyaox)_6(pyaoxH)_6(MeOH)_2Cl_2]Cl_4{\cdot}5MeOH$ (**1**·5MeOH) and $[Ni_{16}(pyaox)_8(pyaoxH)_8(MeOH)_4](SO_4)_4{\cdot}10H_2O{\cdot}26MeOH$ (**2**·10H_2O·26MeOH). The two clusters are high-spin featuring both the singly ($pyaoxH^-$) and doubly deprotonated ($pyaox^{2-}$) forms of $pyaoxH_2$. **2**·10H_2O·26MeOH is the first example of a metal cluster with a quadruple-decker topology, being also the highest nuclearity metal cluster, in general, containing any form of the $pyaoxH_2$ ligand and the highest nuclearity Ni^{II} cluster with any type of 2-pyridyl oxime. In addition, its nuclearity is the highest that has been observed so far in metal clusters bearing 2-pyridyl oximes.[17c,26] The number of the decks in **1**·5MeOH and **2**·10H_2O·26MeOH, and hence the nuclearity of the products, depend on the nature of the inorganic anion that is present in the reaction system, providing elements of synthetic control towards new ferromagnetic species. Portions of this work have been previously communicated.[21]

Experimental section

Materials and physical measurements

All manipulations were performed under aerobic conditions using materials (reagent grade) and solvents as received. The organic ligand $pyaoxH_2$ was synthesized following the reported method.[27] Elemental analyses (C, H, N) were performed by the University of Patras microanalysis service. IR spectra (4000–400 cm^{-1}) were recorded using a Perkin Elmer 16PC FT-IR spectrometer with samples prepared as KBr pellets. The magnetic susceptibility measurements were carried out on a Quantum Design SQUID magnetometer MPMS-XL 7 operating

between 1.8 and 300 K for dc-applied fields ranging from 0 to 5 T. Microcrystalline samples were dispersed in vaseline in order to avoid torquing of the crystallites. The sample mulls were contained in a calibrated gelatin capsule held at the center of a drinking straw that was fixed at the end of the sample rod. Alternating current (ac) susceptibility measurements were carried out under an oscillating ac field of 3.5 Oe and frequencies ranging from 0.1 to 1500 Hz. The heat capacity measurements were carried out for temperatures down to 0.3 K by using a Quantum Design 14T-PPMS, equipped with a ^{3}He cryostat. The experiments were performed on thin pressed pellets (*ca*. 1 mg) of a polycrystalline sample, thermalized by *ca*. 0.2 mg of Apiezon N grease, whose contribution was subtracted by using a phenomenological expression.

Synthetic details

Preparation of the complex $[Ni_{12}(pyaox)_6(pyaoxH)_6(MeOH)_2Cl_2]Cl_4\cdot 5MeOH$ (1·5MeOH). Solid NaOMe (0.054 g, 1.00 mmol) was added to a colourless solution of pyaoxH$_2$ (0.068 g, 0.50 mmol) in MeOH (15 mL); the solid soon dissolved. Solid $NiCl_2\cdot 6H_2O$ (0.119 g, 0.50 mmol) was then added and the resulting slurry was stirred for 15 min at room temperature. The dark brown slurry was filtered and the solution was left to stand undisturbed in a closed flask for a period of 3–4 days. Dark brown crystals appeared which were collected by filtration, washed with H_2O (1 mL), cold EtOH (1 mL) and Et_2O (3 mL), and dried in air. Yield: 60%. The dried solid was analyzed satisfactorily as **1**. Calcd (found): C 34.07 (33.84), H 2.86 (2.90), N 19.33 (19.21) %. IR (KBr, cm^{-1}): 3328b, 1654m, 1608s, 1577m, 1542s, 1483s, 1448w, 1416m, 1303w, 1263w, 1158m, 1103w, 1076m, 1023m, 992w, 938w, 782m, 729w, 702w, 645m, 517w, 480w.

Preparation of the complex $[Ni_{16}(pyaox)_8(pyaoxH)_8(MeOH)_4](SO_4)_4\cdot 10H_2O\cdot 26MeOH$ (2·10H$_2$O·26MeOH). NEt_3 (0.139 mL, 1.00 mmol) was added to a colourless solution of pyaoxH$_2$ (0.068 g, 0.50 mmol) in MeOH (20 mL). Solid $NiSO_4\cdot 6H_2O$ (0.130 g, 0.50 mmol) was then added and the resulting solution was stirred under heating (45 °C) for 15 min. The dark brown solution was left to stand undisturbed in a closed flask for a period of 3–4 days. Dark brown crystals appeared which were collected by filtration, washed with cold EtOH (1 mL) and Et_2O (3 mL), and dried in air. Yield: 65%. The dried solid was analyzed satisfactorily as $2\cdot 8H_2O\cdot 22MeOH$. Calcd (found): C 32.78 (32.52), H 4.69 (4.25), N 15.04 (15.17) %. IR (KBr, cm^{-1}): 3332b, 1654m, 1606m, 1580w, 1542m, 1482m, 1415m, 1300w, 1263w, 1100s, 1022w, 981w, 933w, 777m, 747w, 700w, 646m, 617s, 515w, 468m.

Single-crystal X-ray crystallography

Suitable single-crystals of **1**·5MeOH and $2\cdot 10H_2O\cdot 26MeOH$ were mounted on a Hampton Research CryoLoop using FOMBLIN Y perfluoropolyether vacuum oil (LVAC 25/6) purchased from Aldrich,[28] with the help of a Stemi 2000 stereomicroscope equipped with Carl Zeiss lenses. Data were collected at 150(2) K on a Bruker X8 Kappa APEX II charge-coupled device (CCD) area-detector diffractometer (Mo K_α graphite-monochromated radiation, λ = 0.71073 Å) controlled by the APEX2 software package,[29] and equipped with an Oxford Cryosystems Series 700 cryostream monitored remotely using the software interface, Cryopad.[30] Images were processed using the software package SAINT+,[31] and data were corrected for absorption by the multi-scan semi-empirical method implemented in SADABS.[32] The structures were solved by the direct methods of SHELXS-97,[33] and refined by full-matrix least squares on F^2 using SHELXL-97.[34]

All non-hydrogen atoms were directly located from difference Fourier maps and successfully refined with anisotropic displacement parameters. For both compounds, hydrogen atoms attached to carbon and to the hydroxido groups were located at their idealised positions and included in the structural model in subsequent refinement cycles in riding-motion approximation with U_{iso} = 1.2 (aromatic carbon) or 1.5 (–CH$_3$ and –OH groups) of U_{eq} of the parent atom. Hydrogen atoms associated with the nitrogen atoms were markedly visible in difference Fourier maps and were included in the structures with the N–H and H···H distances restrained to 0.90(1) and 1.50(1) Å, respectively, and with $U_{iso} = 1.5 \times U_{eq}$(N).

For $2\cdot 10H_2O\cdot 26MeOH$ the hydrogen atoms belonging to the uncoordinated water molecules could not be directly located from difference Fourier maps and no attempt was made to place these in approximate calculated positions; they have been included in the empirical formula of the compound.

Beside the solvent molecules located in both the structures (5 MeOH in compound **1**, as well as 10 H_2O and 26 MeOH in **2**), considerable smeared-out electron densities were found in the empty spaces available in the two structures, which prevented a sensible location and refinement of other solvent molecules. A search for the total potential solvent area using the software package *PLATON*[35] revealed the presence of large voids housing the disordered molecules. The two data sets were then analysed using the Squeeze,[36] and the reflection lists arising from this procedure were used for the final structural refinements.

Full details can be found in Table 1 and the cif files.

Results and discussion

Synthetic parameters and IR spectra

Our groups have strong interest in the employment of 2-pyridyl oxime ligands as a route to high nuclearity 3d transition metal clusters and SMMs.[14,17–21] As a part of this program, we recently decided to explore pyaoxH$_2$ in Ni^{II} cluster chemistry. Thus, a variety of experiments were performed to study how the different synthetic parameters affect the identity and/or crystallinity of the isolated product. In particular, treatment of $NiCl_2\cdot 6H_2O$ with one equivalent of pyaoxH$_2$ and two equivalents of NaOMe in MeOH gave a dark brown solution from which the dodecanuclear cluster $[Ni_{12}(pyaox)_6(pyaoxH)_6$

Table 1 Crystallographic data for compounds **1**·5MeOH and **2**·10H_2O·26MeOH

	1·5MeOH	**2**·10H_2O·26MeOH
Formula[a]	$C_{79}H_{94}Cl_6N_{36}Ni_{12}O_{19}$	$C_{126}H_{228}N_{48}Ni_{16}O_{72}S_4$
M_w	2769.12	4635.16
Crystal system	Triclinic	Triclinic
Space group	$P\bar{1}$	$P\bar{1}$
a/Å	14.8718(8)	16.6742(9)
b/Å	15.1738(7)	17.3665(17)
c/Å	15.3809(8)	19.7073(10)
α/°	60.525(2)	106.175(3)
β/°	73.084(3)	113.293(2)
γ/°	69.854(2)	99.202(4)
V/Å^3	2805.3(3)	4792.3(6)
Z	1	1
T/K	150(2)	150(2)
λ[b]/Å	0.71073	0.71073
D_c/g cm^{-3}	1.639	1.606
μ(Mo Kα)/mm^{-1}	2.182	1.672
Reflections collected	147 901	321 514
Independent reflections	14 885	21 715
R_{int}	0.0422	0.0375
R_1[c]	0.0596	0.0461
wR_2[d]	0.2006	0.1148
Goodness of fit on F^2	1.047	1.138
$\Delta\rho$max/min/e Å^{-3}	4.818/−0.908	1.194/−0.700

[a] Including solvent molecules. [b] Graphite monochromator. [c] $R_1 = \sum(|F_o| - |F_c|)/\sum|F_o|$. [d] $wR_2 = [\sum[w(F_o^2 - F_c^2)^2]/\sum[wF_o^2)^2]]^{1/2}$.

$(MeOH)_2Cl_2]Cl_4$·5MeOH (**1**·5MeOH) was obtained in 60% yield. Its formation can be summarized by eqn (1):

$$12NiCl_2\cdot 6H_2O + 12pyaoxH_2 + 18NaOMe \xrightarrow{MeOH} \underset{\mathbf{1}}{[Ni_{12}(pyaox)_6(pyaoxH)_6(MeOH)_2Cl_2]Cl_4} + 18NaCl + 72H_2O + 16MeOH \quad (1)$$

The methoxide ions act as proton acceptors to facilitate formation of $pyaox^{2-}$ and $pyaoxH^-$ ligands. The reaction procedure involved a slight excess of NaOMe over that required by eqn (1), and this might have proven beneficial in shifting a possible equilibrium to the right. The reaction mixtures which lead to **1** should be filtered before crystallization to remove NaCl which is insoluble in MeOH. The product also needs to be washed with a small amount of H_2O to ensure complete removal of NaCl.

The determination of the crystal structure of **1** with single crystal X-ray crystallography revealed that the twelve metal ions have an unprecedented triple-decker topology with each "deck" containing two square planar and two octahedral Ni^{II} atoms. The intriguing structural and magnetic features of **1** (*vide infra*) prompted us to further study this reaction system exploring the ability of $pyaoxH_2$ to deliver other novel polynuclear Ni^{II} compounds. In the context of this investigation, we decided to employ different counterions possessing higher charge than Cl^- hoping that they could stabilize higher nuclearity clusters. Indeed, this turned out to be the case and the treatment of $NiSO_4$·6H_2O with one equivalent of $pyaoxH_2$ and two equivalents of NEt_3 in MeOH gave a dark brown solution from which the higher nuclearity cluster $[Ni_{16}(pyaox)_8(pyaoxH)_8(MeOH)_4](SO_4)_4$ (**2**) was obtained in 65% yield. Its formation can be summarized by eqn (2):

$$16NiSO_4\cdot 6H_2O + 16pyaoxH_2 + 24NEt_3 + 4MeOH \longrightarrow \underset{\mathbf{2}}{[Ni_{16}(pyaox)_8(pyaoxH)_8(MeOH)_4](SO_4)_4} + 12(NHEt_3)_2SO_4 + 96H_2O \quad (2)$$

The reaction mixture which leads to **2** should be heated for a few minutes to facilitate the dissolution of $NiSO_4$·6H_2O (presumably by reaction with the organic ligand) in MeOH. We observed that reactions with small variations in the Ni^{II} : $pyaoxH_2$ ratio gave the same Ni_{16} compound. The nature of the base and the crystallization method are not crucial for the identity of the product and affect only its crystallinity; we were able to isolate **2** (IR evidence) by using a plethora of bases such as NaOMe, NaOH, NH_3 *etc*.

The IR spectra of dried **1**·5MeOH and **2**·10H_2O·26MeOH exhibit a strong broad band at ~3330 cm^{-1} assignable to the ν(OH) vibration of coordinated MeOH molecules, as well as solvent MeOH and H_2O molecules, and to the $\nu(NH_2)/\nu(NH)$ vibrations of the pyaoxH/$pyaox^{2-}$ ligands. The broadness and low frequency of these bands are both indicative of strong hydrogen bonding. There are medium intensity bands at 1566 and 1116 cm^{-1} in the spectrum of the free $pyaoxH_2$ ligand, which are assigned to $\nu(C{=}N)_{oxime}$ and $\nu(N{-}O)_{oxime}$, respectively.[27] The 1116 cm^{-1} band is shifted to a lower wavenumber (1103 cm^{-1} in **1**·5MeOH; 1100 cm^{-1} in **2**·10H_2O·26MeOH). This shift is attributed to the coordination of the oximate nitrogen.[37] The band is strong in the spectrum of the Ni_{16} cluster, because it also has a $\nu_3(F_2)$ [ν_d(SO)] character due to the ionic sulfates (T_d symmetry). Somewhat to our surprise, the 1566 cm^{-1} band is shifted to a higher wavenumber in the complexes (1577 cm^{-1} in **1**·5MeOH, 1580 cm^{-1} in **2**·10H_2O·26MeOH), overlapping with an aromatic stretch. This shift may be indicative of the oximate nitrogen coordination.[37] Extensive studies on Schiff-base complexes (which also contain a C=N bond) have shown[38] that a change in the s character of the nitrogen lone pair occurs upon coordination such that the s character of the nitrogen orbital, which is involved in the C=N bond, increases; this change in hybridization produces a greater C=N stretching force constant relative to the free neutral ligand. The in-plane deformation band of the 2-pyridyl ring of free $pyaoxH_2$ at 632 cm^{-1} shifts upwards in **1**·5MeOH (646 cm^{-1}) and **2**·10H_2O·26MeOH (645 cm^{-1}), confirming the involvement of the ring-N atom in coordination.[39]

Description of structures

Representations of the molecular structure and the structural core of compound **1**·5MeOH are shown in Fig. 1. Selected interatomic distances and angles are listed in Table 2. Compounds **1**·5MeOH and **2**·10H_2O·26MeOH display related structures based on parallel Ni_4 layers, $\{Ni_4(pyaox)_2(pyaoxH)_2\}^{2+}_x$ (x = 3, **1**·5MeOH; x = 4, **2**·10H_2O·26MeOH). Thus,

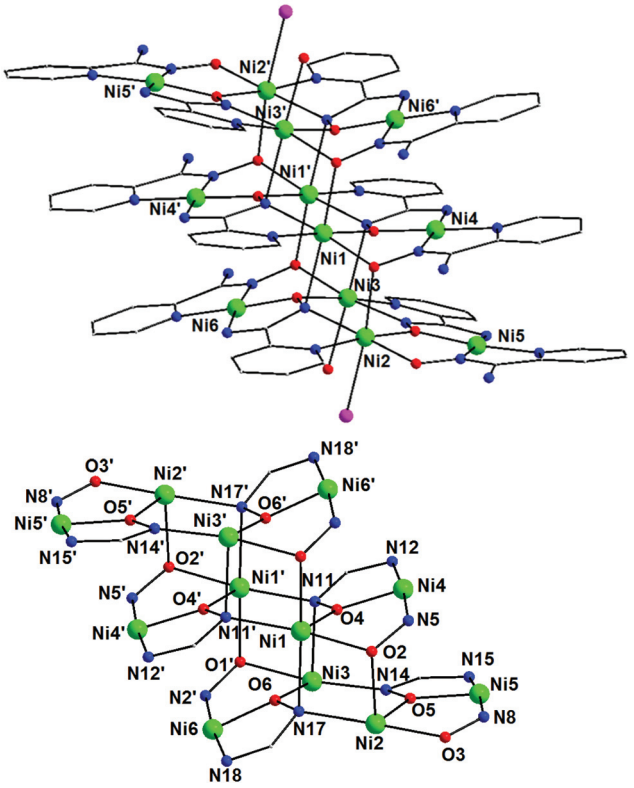

Fig. 1 Representations of the molecular structure of the cation of **1** (top) and its triple-decker structural core (bottom).

Table 2 Selected interatomic distances and angles for **1**·5MeOH[a]

Ni1–O4	2.0279(18)	Ni3–N11	2.250(2)
Ni1–O2	2.0293(19)	Ni4–O4	1.8306(18)
Ni1–N10′	2.048(2)	Ni4–N5	1.853(2)
Ni1–N11′	2.070(2)	Ni4–N12	1.861(2)
Ni1–O1	2.1705(19)	Ni4–N4	1.903(2)
Ni1–N17	2.278(2)	Ni5–O5	1.8263(19)
Ni2–O3	1.998(2)	Ni5–N15	1.846(2)
Ni2–O5	2.0033(19)	Ni5–N8	1.852(2)
Ni2–N16	2.031(2)	Ni5–N7	1.887(2)
Ni2–N17	2.089(2)	Ni6–O6	1.8227(18)
Ni2–O2	2.1729(19)	Ni6–N18	1.846(2)
Ni2–Cl1	2.5713(10)	Ni6–N2′	1.846(2)
Ni3–N14	2.013(2)	Ni6–N1′	1.888(2)
Ni3–O6	2.0320(18)	Ni2⋯Ni3	3.891(2)
Ni3–O1′	2.0589(19)	Ni2⋯Ni5	3.323(2)
Ni3–N13	2.076(2)	Ni2⋯Ni6	4.670(2)
Ni3–O1 M	2.113(2)	Ni1⋯Ni3	3.141(2)
O4–Ni1–N10′	178.74(8)	N5–Ni4–N12	174.14(10)
O2–Ni1–N11′	172.77(8)	O4–Ni4–N4	172.22(9)
O1–Ni1–N17	175.06(7)	N12–Ni4–N4	102.89(10)
O5–Ni2–N16	175.01(9)	N15–Ni5–N8	173.30(11)
O2–Ni2–Cl1	172.98(5)	O5–Ni5–N7	170.12(10)
O3–Ni2–N17	169.24(8)	N15–Ni5–N7	102.09(11)
O6–Ni3–N13	173.75(9)	N18–Ni6–N2′	174.26(10)
O1M–Ni3–N11	172.46(9)	O6–Ni6–N1′	172.83(10)
N14–Ni3–N11	89.73(9)	N18–Ni6–N1′	102.40(10)

[a] Symmetry transformations used to generate equivalent atoms: ′: $-x$, $-y$, $-z+1$.

only the structure of compound **1**·5MeOH will be discussed in detail and compared to that of **2**·10H_2O·26MeOH.

Complex **1**·5MeOH crystallizes in the triclinic space group $P\bar{1}$. Its structure consists of $[Ni_{12}(pyaox)_6(pyaoxH)_6Cl_2(MeOH)_2]^{4+}$ cations, Cl^- counterions and MeOH lattice molecules. The centrosymmetric cation of **1**·5MeOH is composed of six distorted octahedral (Ni1, Ni2, Ni3 and symmetry equivalents) and six square planar (Ni4, Ni5, Ni6 and symmetry equivalents) Ni^{II} atoms, which are held together through two $\eta^1{:}\eta^1{:}\eta^1{:}\mu$ and four $\eta^1{:}\eta^1{:}\eta^2{:}\mu_3$ $pyaoxH^-$ ligands, as well as two $\eta^1{:}\eta^1{:}\eta^1{:}\eta^2{:}\mu_3$ and four $\eta^1{:}\eta^2{:}\eta^1{:}\eta^2{:}\mu_4$ $pyaox^{2-}$ groups (Scheme 2). The coordination sphere of the Ni^{II} atoms is completed by two terminal chlorido ligands on Ni2 and Ni2′, and two terminal MeOH molecules on Ni3 and Ni3′. The twelve metal ions in **1**·5MeOH are arranged into three layers, which are stacked one above the other forming an unusual, for 3d-metal cluster chemistry, triple-decker topology. Each "deck" contains two square planar and two octahedral Ni^{II} atoms, whereas the linkage of the central deck with each of the outer decks is achieved through two bridging oxygen atoms from two $\eta^1{:}\eta^1{:}\eta^2{:}\mu_3$ $pyaoxH^-$ ligands and two bridging oximate nitrogen atoms from two $\eta^1{:}\eta^2{:}\eta^1{:}\eta^2{:}\mu_4$ $pyaox^{2-}$ groups. The four Ni^{II} atoms of the two outer layers are arranged in an almost planar topology with the largest deviation from the plane being 0.14 Å for Ni3 and Ni6, whereas the metal ions in the central layer are perfectly coplanar. The distance between two adjacent decks is ~2.70 Å. The chromophores in **1**·5MeOH are $Ni(1,1')(N_{py})(N_{ox})_2(O_{ox})_3$, $Ni(2,2')(N_{py})(N_{ox})(O_{ox})_3(Cl)$, $Ni(3,3')(N_{py})(N_{ox})_2(O_{ox})_2(O_{MeOH})$ and $Ni(4,4'/5,5'/6,6')(N_{py})(N_{ox})(N_{am})(O_{ox})$, where the abbreviations "py", "ox" and "am" are for the 2-pyridyl, oximate and deprotonated amino donor atoms, respectively. The strong ligand field, deprotonated amino donor atoms are coordinated only to the square planar Ni^{II} atoms and may be considered responsible for their geometry. The average Ni(4,5,6)-N_{py}, N_{ox}, O_{ox} bond distances are 1.893, 1.850 and 1.827 Å, respectively, while the average Ni(1,2,3)–N_{py}, N_{ox}, O_{ox} bond lengths are 2.052, 2.140 and 2.062 Å, respectively. The longer bonds involving Ni(1,2,3) compared to those involving Ni(4,5,6) are a consequence of the higher coordination number of Ni1, Ni2 and Ni3.

The $\eta^1{:}\eta^2{:}\eta^1{:}\eta^2{:}\mu_4$ coordination mode of $pyaox^{2-}$ found in **1**·5MeOH is extremely rare in the coordination chemistry of pyridine-2-amidoxime.[21] In fact, this can be rationalised by considering the C–N_{ox} bond lengths; the C–N_{ox} and C–N_{am} distances for the $\eta^1{:}\eta^2{:}\eta^1{:}\eta^2{:}\mu_4$ $pyaox^{2-}$ ligands (average values: 1.345 and 1.322 Å) are longer and shorter, respectively, than those for the $\eta^1{:}\eta^1{:}\eta^1{:}\eta^2{:}\mu_3$ $pyaox^{2-}$ ligands (1.318 and 1.336 Å),

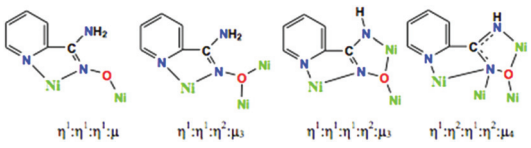

Scheme 2 The crystallographically established coordination modes of $pyaoxH^-$ and $pyaox^{2-}$ in complexes **1** and **2**.

indicating a decreased double bond character for the C–N_{ox} bond and an increased double bond character for the C–N_{am} bond in the former.

The crystal structure of **1**·5MeOH is stabilized by strong intramolecular hydrogen bonds between the O atoms of the terminally ligated MeOH molecules (O1M), which act as donors, and the terminal chlorido ligands, which act as acceptors [O1 M···Cl1 = 3.199(2) Å, H1 M···Cl1 = 2.256(2) Å, O1 M–H1 M–Cl1 = 167.19(2)°]. In addition, there is a network of intermolecular H bonds that involve: (1) the Cl^- counterions (acceptors) and the NH_2 groups (donors) of the organic ligands [N3···Cl3 = 3.245(2), H3B···Cl3 = 2.360(2) Å, N3–H3B–Cl3 = 166.93°; N9···Cl3 = 3.282(2) Å, H9B···Cl3 = 2.421(2) Å, N9–H9B–Cl3 = 159.83°] resulting in the formation of 1D chains, and 2) the coordinated chlorido ligands (acceptor) and the MeOH lattice molecules (donors) [O3 M···Cl1 = 3.237(2) Å, H9 M···Cl1 = 2.422(2) Å, O3 M–H9 M–Cl1 = 163.49°]. The cations of **1** are in close proximity with the shortest metal···metal separation between the adjacent Ni_{12} units being 4.797(2) Å (Ni5···Ni5).

Representations of the molecular structure and the structural core of compound **2**·10H_2O·26MeOH are shown in Fig. 2. Selected interatomic distances and angles are listed in Table S1 in the ESI.†

Complex **2**·10H_2O·26MeOH crystallizes in the triclinic space group $P\bar{1}$. Its structure consists of $[Ni_{16}(pyaox)_8(pyaoxH)_8(MeOH)_4]^{8+}$ cations, SO_4^{2-} counterions, and MeOH and H_2O lattice molecules. Similarly to **1**·5MeOH, the Ni^{II} atoms in **2**·10H_2O·26MeOH are stacked in four layers, which form an unprecedented quadruple-decker topology. In particular, the inner decks in **2**·10H_2O·26MeOH are identical with the central deck of **1**·5MeOH; thus, figuratively speaking, an internal deck has been added to the Ni_{12} cation of the latter to form a Ni_{16} cluster (**2**·10H_2O·26MeOH). In addition, the external decks in **2**·10H_2O·26MeOH are similar to the corresponding decks in **1**·5MeOH, with their only difference being the replacement of the chlorido ligands in the latter by terminal MeOH molecules in the former. The octahedral metal centres are Ni1, Ni2, Ni3 and Ni4 (and their symmetry equivalents) and the square planar ones are Ni5, Ni6, Ni7 and Ni8 (and their symmetry equivalents). The presence of many lattice molecules and counterions in the crystal structure of **2**·10H_2O·26MeOH results in the formation of a network of strong intermolecular hydrogen bonding interactions. Details of these interactions are listed in Table S2 in the ESI.† As it was the case for **1**·5MeOH, the cations of **2**·10H_2O·26MeOH, are in close proximity with the shortest metal···metal separation between the adjacent Ni_{16} units being 4.671(2) Å (Ni1···Ni7).

1·5MeOH and **2**·10H_2O·26MeOH are new additions in the small family of high nuclearity, high spin Ni compounds with multiple-decker metal topology.[23,24] In particular, **2**·10H_2O·26MeOH is the first structurally characterized complex of any metal displaying a quadruple-decker configuration. Compound **1**·5MeOH can be described as a "trimer-of-tetramers", while **2**·10H_2O·26MeOH as a "tetramer-of tetramers", where the tetramer in both cases is the structural unit

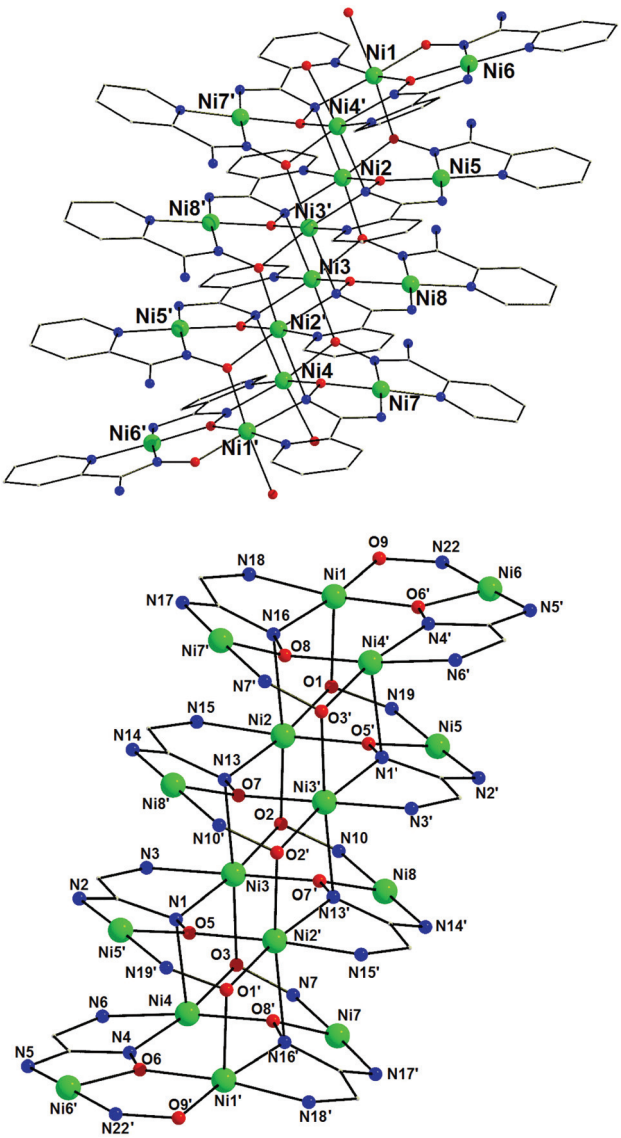

Fig. 2 Representations of the molecular structure of the cation of **2** (top) and its quadruple-decker structural core (bottom).

$\{Ni_4(pyaox)_2(pyaoxH)_2\}^{2+}$, which has been previously observed in a discrete tetranuclear cluster.[23,24] The number of the decks, and hence the nuclearity and spin, of **1**·5MeOH and **2**·10H_2O·26MeOH is affected by the nature (charge, shape) of the inorganic anion that is present in the reaction system providing the elements of synthetic control towards new high nuclearity Ni^{II} clusters. Both compounds contain the singly and doubly deprotonated pyridine-2-amidoxime ligand, with **2**·10H_2O·26MeOH being (1) the highest nuclearity metal cluster bearing this ligand, (2) one of the few highest nuclearity hexadecanuclear metal clusters with any 2-pyridyl oxime, in general,[17c,26] and (3) the highest nuclearity Ni^{II} cluster with 2-pyridyl oximes. Furthermore, complex **2**·10H_2O·26MeOH joins only a very small family of Ni_{16} clusters with O- or/and N-ligation.[40]

Magnetic susceptibility studies

In order to probe the magnetic properties of the clusters, direct current (dc) magnetic susceptibility measurements were performed on polycrystalline samples of compounds **1** and **2** in the temperature range 2–300 K, with an applied magnetic field of 0.1 T.

The collected data are plotted as $\chi_M T$ *versus* T in Fig. 3, which reveal room-temperature $\chi_M T$ values of 7.16 and 9.03 cm^3 K mol^{-1} for **1** and **2**, respectively. These are in good agreement with the $\chi_M T$ value expected (g = 2.10) for six non-interacting octahedral Ni^{II} ions (6.615 cm^3 mol^{-1} K) in **1**, and eight non-interacting octahedral Ni^{II} ions (8.82 cm^3 mol^{-1} K) in **2**. For both compounds, the value of $\chi_M T$ steadily increases to a maximum value (14.5 cm^3 mol^{-1} K at 14 K, **1**; 21.7 cm^3 mol^{-1} K at 10 K, **2**), and then sharply decreases to 10.8 and 14.0 cm^3 mol^{-1} K at 2.0 K for **1** and **2**, respectively. The profile of the $\chi_M T$ *versus* T plots is indicative of dominant ferromagnetic interactions between the paramagnetic ions within the cations of **1** and **2**. The low temperature decrease of the $\chi_M T$ value is attributed to intermolecular antiferromagnetic interactions and/or zero-field splitting. The former is consistent with the crystal structure of the two compounds (*vide supra*).

In order to fit the $\chi_M T$ data for **1**·5MeOH, we modeled the Ni_6 magnetic core with the 2J-model described in Fig. 4, left, (the octahedral Ni^{II} atoms define two triangles related by an inversion centre) employing the isotropic spin-Hamiltonian (1):

$$\begin{aligned}\hat{H} = &-2J_1(\hat{S}_1\cdot\hat{S}_3 + \hat{S}_1\cdot\hat{S}_{1'} + \hat{S}_2\cdot\hat{S}_3 + \hat{S}_{1'}\cdot\hat{S}_{3'} + \hat{S}_{2'}\cdot\hat{S}_{3'}) \\ &-2J_2(\hat{S}_1\cdot\hat{S}_2 + \hat{S}_1\cdot\hat{S}_{3'} + \hat{S}_{1'}\cdot\hat{S}_3 + \hat{S}_{1'}\cdot\hat{S}_{2'}) + \Sigma_i\mu_B g_{Ni}\vec{H}\hat{S}_i\end{aligned} \quad (1)$$

where J is the isotropic exchange interaction parameter, i is the index for each Ni^{II} ion in the Ni_6 core, μ_B is the Bohr magneton, g_{Ni} = 2.10, the g-factor of the Ni^{II} ions, B is the applied magnetic field and $\hat{S}$ is a spin operator. The data was numerically fitted using the simplex algorithm,[41] with intermolecular interactions being taken into account in the frame of mean-field theory, by the use of the Curie–Weiss temperature, θ. The fit affords the parameters J_1 = +5.14 cm^{-1}, J_2 = +3.01 cm^{-1} and θ = −5.73 K. This results in an S = 6 ground state with the nearest excited states being S = 5, lying 8.38 cm^{-1} higher in energy, and S = 4, lying at 17.11 cm^{-1}. A plot of energy *versus* the total spin state is given in Fig. S1, left, in the ESI.† Similarly, the 2J-model described in Fig. 4, right, was used in order to fit the data for the Ni_8 magnetic core of **2**·10H_2O·26MeOH using the isotropic spin-Hamiltonian (2):

$$\begin{aligned}\hat{H} = &-2J_1(\hat{S}_1\cdot\hat{S}_{4'} + \hat{S}_2\cdot\hat{S}_{3'} + \hat{S}_2\cdot\hat{S}_{4'} + \hat{S}_3\cdot\hat{S}_{3'} + \hat{S}_{1'}\cdot\hat{S}_4 + \hat{S}_{2'}\cdot\hat{S}_3 + \hat{S}_{2'}\cdot\hat{S}_4) \\ &-2J_2(\hat{S}_1\cdot\hat{S}_2 + \hat{S}_2\cdot\hat{S}_3 + \hat{S}_3\cdot\hat{S}_4 + \hat{S}_{1'}\cdot\hat{S}_{2'} + \hat{S}_{2'}\cdot\hat{S}_{3'} + \hat{S}_{3'}\cdot\hat{S}_{4'}) \\ &+\Sigma_i\mu_B g_{Ni}\vec{H}\hat{S}_i\end{aligned} \quad (2)$$

The fit afforded the parameters J_1 = +5.45 cm^{-1}, J_2 = +2.00 cm^{-1} and θ = −3.43 K. This results in an S = 8 ground state with the nearest excited states being S = 7 (3.95 cm^{-1}) and S = 6 (8.07 cm^{-1}) lying relatively close in energy, Fig. S1,† right. We have also collected the alternating current (ac) magnetic susceptibility in zero applied dc field for both complexes, which revealed no frequency dependence (Fig. S2 in the ESI†).

Fig. S3 in the ESI† shows the dc-field magnetization data $M(H)$ collected in the range 0–7 T at three temperatures between 2.3 and 20 K for **1** and **2**. In both cases, $M(H)$ initially rises quickly at the lowest temperatures, as expected for ferromagnetic exchange, and then keeps increasing slowly even at the highest applied fields, without reaching saturation. In accordance with the susceptibility data, this behaviour is attributed to intermolecular antiferromagnetic interactions, likely combined with some degree of magnetic anisotropy. For comparison, the calculated Brillouin curves were also plotted assuming uncorrelated molecules with S = 6 (**1**) and S = 8 (**2**) for the representative temperatures. For both compounds, it is observed that the experimental data tend to lie below the calculated curve, suggesting the influence either from antiferromagnetic intermolecular correlations or from low-lying excited spin states. The latter is more evident in **2** with respect to **1**, as it is revealed from the larger deviation of the calculated curve and experimental data, which indicates that **2** does not display a well-defined ground state spin value. Keeping the values of S and g stable, detectable improvements are obtained only by adding an abnormally high uniaxial magnetic anisotropy term D in the case of **1**. Since this applies also at the lowest

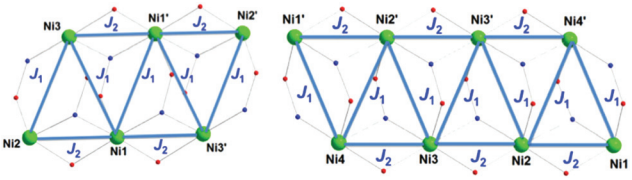

Fig. 4 Schematic presentation of the coupling scheme used to model susceptibility data for the cations of **1** (left) and **2** (right).

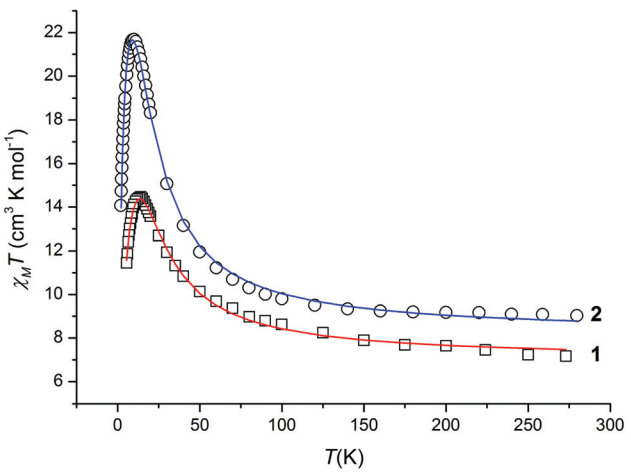

Fig. 3 Plot of $\chi_M T$ as a function of T for complexes **1** (□) and **2** (○); the solid lines represent the fit of the data to the theoretical models given in the text.

investigated temperatures, in which the influence of excited states should be negligible, we conclude, in agreement with the susceptibility data, that antiferromagnetic interactions between cations are important for the two complexes.

It has recently been reported that the dominant factor which affects the magnetic properties of the oximato Ni^{II} compounds is the length of the bridging N–O bond.[23,42] In particular, DFT calculations on an oximato bridged Ni^{II} compound revealed that N–O distances larger than 1.394 Å result in ferromagnetic interactions, while shorter ones propagate antiferromagnetic interactions. This observation has been explained by considering that with the decrease of the N–O bond, the spin population on the N and O atoms increases, thus enhancing the antiferromagnetic coupling between Ni^{II} ions. In compounds **1**·5MeOH and **2**·10H_2O·26MeOH, the N–O distances are in the range of 1.401–1.425 Å, and thus the experimentally obtained ferromagnetic interactions are in excellent agreement with the previously reported theoretical calculations.

Specific heat measurements

Fig. 5 shows the collected specific heat $C(T,H)$ data of **1** as a function of temperature for several applied fields. No particular feature is detected except for a very broad anomaly around 2 K at zero applied field, whose magnetic nature is proven by the fact that it quickly moves towards higher temperatures as the field H is increased. As typical for molecule-based materials,[43] the contribution to the total C arising from lattice vibrations dominates as T increases above that of liquid helium.

The lattice contribution can be described by the Debye model (dashed line in Fig. 5), which simplifies to a $C/R = aT^3$ dependence (R is the gas constant) at the lowest temperatures, where $a = 3.9 \times 10^{-3}$ K^{-3} for **1**. The magnetic contribution C_m (see inset in Fig. 5) is then obtained by subtracting the lattice contribution to the total C. This analysis reveals a bump centered at ≈9 K, that we associate with a Schottky-like anomaly, *i.e.*, crystal-field splitting of the $S = 6$ multiplet. By decreasing the temperature, magnetic fluctuations within the 2D layers show up in the anomaly centered at ≈2 K. To properly associate these features with the magnetic contribution, we estimate the zero-field magnetic entropy $S_m = \int C_m/T dT$, shown in Fig. S4 in the ESI.† This tends at high-T to the value of 2.8 R, which is in fair agreement with the magnetic entropy expected, $R \ln(2S + 1) = 2.56\ R$ (provided the spin value is $S = 6$) and consistent with the magnetization data. Since the lattice contribution is sensibly larger than C_m, the latter is affected by an important uncertainty. This inhibits us from providing anything other than a qualitative analysis of the experimental data.

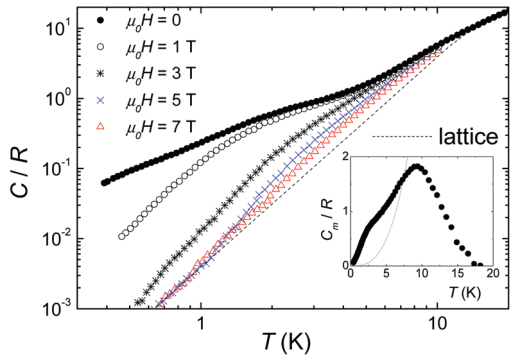

Fig. 5 Specific heat C for **1** normalised to the gas constant R *vs.* T in the indicated temperature and field ranges. Inset: Magnetic contribution C_m as obtained by subtracting the lattice contribution (dashed line) to C.

Specific heat data have been also collected for **2** and these are shown in Fig. S5 in the ESI† as a function of temperature for several applied magnetic fields. As it is the case for **1**, the specific heat at high temperatures is dominated by a non-magnetic contribution, which is due to the thermal vibrations of the lattice. Furthermore, there is a clear magnetic contribution, which extends over a broad temperature range, *i.e.*, from the lowest accessed T to well inside the range mainly determined by the lattice contribution to the specific heat. The fact that **2** does not display a well-defined ground state spin value ($S \approx 8$, *vide supra*) prevents to determine reliably the magnetic contribution by subtracting the lattice specific heat from the total measured signal, as in the case of the Ni_{12} complex. As a result, a valuable analysis of the specific heat data is not feasible for **2**.

Conclusions

The employment of $pyaoxH_2$ in Ni^{II} chemistry has provided access to the new multiple-decker Ni complexes $[Ni_{12}(pyaox)_6(pyaoxH)_6(MeOH)_2Cl_2]Cl_4$·5MeOH (**1**·5MeOH) and $[Ni_{16}(pyaox)_8(pyaoxH)_8(MeOH)_4](SO_4)_4$·10$H_2O$·26MeOH (**2**·10$H_2O$·26MeOH) comprising stacked Ni_4 layers, $\{Ni_4(pyaox)_2(pyaoxH)_2\}^{2+}_x$ ($x = 3$, **1**·5MeOH; $x = 4$, **2**·10H_2O·26MeOH), with each layer containing two square planar and two octahedral Ni^{II} centres.

Compound **1**·5MeOH is a new addition to the small family of Ni_{12} clusters with a triple-decker topology.[23,24] Compound **2**·10H_2O·26MeOH displays a quadruple-decker configuration, which has never been observed before in metal cluster chemistry. In addition, **2**·10H_2O·26MeOH is the highest nuclearity metal cluster bearing $pyaoxH_2$ and joins only a very small family of Ni_{16} clusters with O- or/and N-ligation. It also belongs to the very small family of the hexadecanuclear homometallic or/and heterometallic clusters, which display the highest nuclearity that has been observed so far for compounds containing 2-pyridyl oximes, being the only Ni^{II} cluster in this category.[17c,25]

Dc and ac magnetic susceptibility and heat capacity measurements were performed on **1** and **2**, which revealed that both display ferromagnetic exchange interactions resulting in a spin ground state of $S = 6$ for **1** and $S = 8$ for **2**. Intercationic interactions, as revealed by single crystal X-ray crystallography, affect the magnetic properties preventing an in-depth analysis of the heat capacity measurements.

The number of decks in **1** and **2** is affected by the use of different inorganic anions with the bulkier and of a higher charge anion (SO_4^{2-} *vs.* Cl^-) being able to stabilize the higher nuclearity cluster. This could lead to the development of a rational method towards the increase of the nuclearity and the spin of ferromagnetic species. Based on this, we believe that we have seen just the tip of the iceberg in the Ni^{II}/pyaoxH_2 compounds with a multiple decker topology. We have every reason to believe that higher nuclearity such species (*e.g.*, Ni_{20}, Ni_{24}, *etc.*) are waiting to be discovered. Further studies towards this direction are currently in progress including the employment of higher charge counterions (*e.g.*, PO_4^{3-}). These studies will be reported in due course.

Acknowledgements

CP and CE thank the School of Chemistry, NUI Galway, for the financial support. RI thanks the Royal Society of Edinburgh and ME thanks Spanish MINECO (MAT2015-68204-R) for funding. LCS acknowledges the financial support by FEDER (Fundo Europeu de Desenvolvimento Regional) through PT2020, by FCT (Fundação para a Ciência e a Tecnologia) for the research centre REQUIMTE/LAQV (UID/QUI/50006/2013) and for the grant SFRH/BPD/111899/2015.

Notes and references

1 (*a*) R. Sessoli, H. L. Tsai, A. R. Schake, S. Wang, J. B. Vincent, K. Folting, D. Gatteschi, G. Christou and D. N. Hendrickson, *J. Am. Chem. Soc.*, 1993, **115**, 1804; (*b*) R. Sessoli, D. Gatteschi, A. Caneschi and M. A. Novak, *Nature*, 1993, **365**, 141.

2 For reviews and books, see: (*a*) R. Bagai and G. Christou, *Chem. Soc. Rev.*, 2009, **38**, 1011; (*b*) C. Papatriantafyllopoulou, E. Moushi, G. Christou and A. J. Tasiopoulos, *Chem. Soc. Rev.*, 2016, **45**, 1597; (*c*) M. Murrie and D. J. Price, *Annu. Rep. Prog. Chem.*, 2007, **103**, 20; (*d*) G. Aromi and E. K. Brechin, *Struct. Bonding*, 2006, **122**, 1; (*e*) D. Gatteschi, R. Sessoli and J. Villain, *Molecular Nanomagnets*, Oxford University Press, Oxford, 2006; (*f*) C. J. Milios and R. E. P. Winpenny, *Struct. Bonding*, 2015, **164**, 1.

3 (*a*) M. Affronte, *J. Mater. Chem.*, 2009, **19**, 1731; (*b*) L. Bogani and W. Wernsdorfer, *Nat. Mater.*, 2008, **7**, 179.

4 (*a*) G. A. Timco, T. B. Faust, F. Tuna and R. E. P. Winpenny, *Chem. Soc. Rev.*, 2011, **40**, 3067; (*b*) P. C. E. Stamp and A. Gaita-Ariño, *J. Mater. Chem.*, 2009, **19**, 1718.

5 (*a*) S. Hill, R. S. Edwards, N. Aliaga-Alcalde and G. Christou, *Science*, 2003, **302**, 1015; (*b*) R. Tiron, W. Wernsdorfer, D. Foguet-Albiol, N. Aliaga-Alcalde and G. Christou, *Phys. Rev. Lett.*, 2003, **91**, 227203 (1–4).

6 (*a*) A. Kovalev, L. Hayden, G. Bauer and Y. Tscherkovniak, *Phys. Rev. Lett.*, 2011, **106**, 147203; (*b*) D. A. Garanin and E. Chudnovsky, *Phys. Rev.*, 2011, **1**, 011005; (*c*) M. Ganzhorn, S. Klyatskaya, M. Ruben and W. Wernsdorfer, *Nat. Nanotechnol.*, 2013, **8**, 166.

7 (*a*) W. Wernsdorfer, S. Bhaduri, C. Boskovic, G. Christou and D. N. Hendrickson, *Phys. Rev. B: Condens. Matter*, 2002, **65**, 180403; (*b*) W. Wernsdorfer, N. E. Chakov and G. Christou, *Phys. Rev. Lett.*, 2005, **95**, 037203.

8 (*a*) G. Gatteschi and R. Sessoli, *Angew. Chem., Int. Ed.*, 2003, **42**, 268; (*b*) E. Del Barco, A. D. Kent, S. Hill, J. M. North, N. S. Dalal, E. M. Rumberger, D. N. Hendrickson, N. E. Chakov and G. Christou, *J. Low Temp. Phys.*, 2005, **140**, 119; (*c*) P. C. E. Stamp, *Nature*, 1996, **383**, 125.

9 (*a*) W. Wernsdorfer and R. Sessoli, *Science*, 1999, **284**, 133; (*b*) W. Wernsdorfer, M. Soler, G. Christou and D. N. Hendrickson, *J. Appl. Phys.*, 2002, **91**, 7164.

10 (*a*) J. D. Rinehart and J. R. Long, *Chem. Sci.*, 2011, **2**, 2078, and references therein; (*b*) D. N. Woodruff, R. E. P. Winpenny and R. A. Layfield, *Chem. Rev.*, 2013, **113**, 5110; (*c*) K. R. Meihaus and J. R. Long, *Dalton Trans.*, 2015, **44**, 2517 (Perspective).

11 (*a*) A. Ferguson, J. Lawrence, A. Parkin, J. Sanchez-Benitez, K. V. Kamenev, E. K. Brechin, W. Wernsdorfer, S. Hill and M. Murrie, *Dalton Trans.*, 2008, 6409; (*b*) E.-C. Yang, W. Wernsdorfer, L. N. Zakharov, Y. Karaki, A. Yamaguchi, R. M. Isidoro, G.-D. Lu, S. A. Wilson, A. L. Rheingold, H. Isimoto and D. N. Hendrickson, *Inorg. Chem.*, 2006, **45**, 529; (*c*) A. Bell, G. Aromi, S. J. Teat, W. Wernsdorfer and R. E. P. Winpenny, *Chem. Commun.*, 2005, 2808; (*d*) M. Moragues-Cánovas, M. Helliwell, L. Ricard, E. Riviére, W. Wernsdorfer, E. Brechin and T. Mallah, *Eur. J. Inorg. Chem.*, 2004, 2219; (*e*) E.-C. Yang, W. Wernsdorfer, S. Hill, R. S. Edwards, M. Nakano, S. Maccagano, L. N. Zakharov, A. L. Rheingold, G. Christou and D. N. Hendrickson, *Polyhedron*, 2003, **22**, 1727; (*f*) S. T. Ochseinbein, M. Murrie, E. Rusanov, H. Stoeckli-Evans, C. Sekine and H.-U. Güdel, *Inorg. Chem.*, 2002, **41**, 5133; (*g*) H. Andres, R. Basler, A. J. Blake, C. Cadiou, G. Chabboussant, C. M. Grant, H.-U. Güdel, M. Murrie, S. Parsons, C. Paulsen, F. Semadini, V. Villar, W. Wernsdorfer and R. E. P. Winpenny, *Chem. – Eur. J.*, 2002, **8**, 4867.

12 S. Carretta, P. Santini, G. Amorretti, M. Affronte, A. Candini, A. Chirri, I. S. Tidmarsh, R. H. Laye, R. Shaw and E. J. L. McInnes, *Phys. Rev. Lett.*, 2006, **97**, 207201.

13 (*a*) P. Chaudhuri, *Coord. Chem. Rev.*, 2003, **243**, 143; (*b*) A. J. L. Pombeiro and V. Yu Kukushkin, in *Comprehensive Coordination Chemistry II*, ed. J. A. McCleverty and T. J. Meyer, Elsevier, Amsterdam, 2004, vol. 7, pp. 631–637; (*c*) C. J. Milios, S. Piligkos and E. K. Brechin, *Dalton Trans.*, 2008, 1809 (Perspective); (*d*) T. Pathmalingam, S. I. Gorelsky, T. J. Burchell, A.-C. Bédard, A. M. Beauchemin, R. Clérac and M. Murugesu, *Chem. Commun.*, 2008, 2782; (*e*) C. J. Milios, A. Vinslava, W. Wernsdorfer, S. Moggach, S. Parsons, S. P. Perlepes, G. Christou and E. K. Brechin, *J. Am. Chem. Soc.*, 2007, **129**, 2754; (*f*) L. F. Jones, A. Prescimone, M. Evangelisti and E. K. Brechin, *Chem. Commun.*, 2009, 2023.

14 For a comprehensive review, see: C. J. Milios, T. C. Stamatatos and S. P. Perlepes, *Polyhedron*, 2006, **25**, 134 (Polyhedron Report).

15 (*a*) H. Kumagai, M. Endo, M. Kondo, S. Kawata and S. Kitagawa, *Coord. Chem. Rev.*, 2003, **237**, 197; (*b*) C. J. Milios, P. Kyritsis, C. P. Raptopoulou, A. Terzis, R. Vicente, A. Escuer and S. P. Perlepes, *Dalton Trans.*, 2005, 501; (*c*) K. F. Konidaris, C. D. Polyzou, G. E. Kostakis, A. J. Tasiopoulos, O. Roubeau, S. J. Teat, E. Manessi-Zoupa, A. K. Powell and S. P. Perlepes, *Dalton Trans.*, 2012, **41**, 2862.

16 (*a*) T. C. Stamatatos, D. Foguet-Albiol, C. C. Stoumpos, C. P. Raptopoulou, A. Terzis, W. Wernsdorfer, S. P. Perlepes and G. Christou, *Polyhedron*, 2007, **26**, 2165; (*b*) T. C. Stamatatos, D. Foguet-Albiol, C. C. Stoumpos, C. P. Raptopoulou, A. Terzis, W. Wernsdorfer, S. P. Perlepes and G. Christou, *J. Am. Chem. Soc.*, 2005, **127**, 15380; (*c*) A. Escuer, G. Vlahopoulou and F. A. Mautner, *Inorg. Chem.*, 2011, **50**, 2717; (*d*) A. M. Mowson, T. N. Nguyen, K. A. Abboud and G. Christou, *Inorg. Chem.*, 2013, **52**, 12320; (*e*) T. Nguyen, W. Wernsdorfer, K. A. Abboud and G. Christou, *J. Am. Chem. Soc.*, 2011, **133**, 20688; (*f*) T. N. Nguyen, M. Shiddiq, T. Ghosh, K. A. Abboud, S. Hill and G. Christou, *J. Am. Chem. Soc.*, 2015, **137**, 7160; (*g*) T. N. Nguyen, W. Wernsdorfer, M. Shiddiq, K. A. Abboud, S. Hill and G. Christou, *Chem. Sci.*, 2016, **7**, 1156.

17 (*a*) T. C. Stamatatos, A. Escuer, K. A. Abboud, C. P. Raptopoulou, S. P. Perlepes and G. Christou, *Inorg. Chem.*, 2008, **47**, 11825; (*b*) T. C. Stamatatos, K. A. Abboud, S. P. Perlepes and G. Christou, *Dalton Trans.*, 2007, 3861; (*c*) C. Papatriantafyllopoulou, T. C. Stamatatos, C. G. Efthymiou, L. Cunha-Silva, F. A. A. Paz, S. P. Perlepes and G. Christou, *Inorg. Chem.*, 2010, **49**, 9743; (*d*) S. Zhang, L. Zhen, B. Xu, R. Inglis, K. Li, W. Chen, Y. Zhang, K. F. Konidaris, S. P. Perlepes, E. K. Brechin and Y. Li, *Dalton Trans.*, 2010, 3563; (*e*) T. C. Stamatatos, C. Papatriantafyllopoulou, E. Katsoulakou, C. P. Raptopoulou and S. P. Perlepes, *Polyhedron*, 2007, **26**, 1830.

18 (*a*) C. D. Polyzou, H. Nikolaou, C. Papatriantafyllopoulou, V. Psycharis, A. Terzis, C. P. Raptopoulou, A. Escuer and S. P. Perlepes, *Dalton Trans.*, 2012, 13755; (*b*) C. Papatriantafyllopoulou, G. Aromi, A. J. Tasiopoulos, V. Nastopoulos, C. P. Raptopoulou, S. J. Teat, A. Escuer and S. P. Perlepes, *Eur. J. Inorg. Chem.*, 2007, 2761; (*c*) C. G. Efthymiou, C. P. Raptopoulou, A. Terzis, S. P. Perlepes, A. Escuer and C. Papatriantafyllopoulou, *Polyhedron*, 2010, **29**, 627; (*d*) C. Papatriantafyllopoulou, M. Estrader, C. G. Efthymiou, D. Dermitzaki, K. Gkotsis, A. Terzis, C. Diaz and S. P. Perlepes, *Polyhedron*, 2009, **28**, 1652; (*e*) D. Dermitzaki, C. P. Raptopoulou, V. Psycharis, A. Escuer, S. P. Perlepes and T. C. Stamatatos, *Dalton Trans.*, 2014, 14520; (*f*) C. Papatriantafyllopoulou, C. P. Raptopoulou, A. Terzis, J. F. Janssens, S. P. Perlepes and E. Manessi-Zoupa, *Z. Naturforsch., B: Chem. Sci.*, 2007, **62**, 1123.

19 (*a*) C. G. Efthymiou, A. A. Kitos, C. P. Raptopoulou, A. Escuer, S. P. Perlepes and C. Papatriantafyllopoulou, *Polyhedron*, 2009, **28**, 3177; (*b*) C. Papatriantafyllopoulou, C. G. Efthymiou, C. Raptopoulou, A. Terzis, E. Manessi-Zoupa and S. P. Perlepes, *Spectrochim. Acta, Part A*, 2008, **70**, 718; (*c*) C. Papatriantafyllopoulou, T. C. Stamatatos, W. Wernsdorfer, S. J. Teat, A. J. Tasiopoulos, A. Escuer and S. P. Perlepes, *Inorg. Chem.*, 2010, **49**, 10486.

20 (*a*) E. Moushi, C. G. Efthymiou, S. P. Perlepes and C. Papatriantafyllopoulou, *Int. J. Inorg. Chem.*, 2011, 606271; (*b*) T. C. Stamatatos, E. Diamantopoulou, C. P. Raptopoulou, V. Psycharis, A. Escuer and S. P. Perlepes, *Inorg. Chem.*, 2007, **46**, 2350.

21 C. Papatriantafyllopoulou, L. F. Jones, T. D. Nguyen, N. Matamoros-Salvador, L. Cunha-Silva, F. A. Almeida Paz, J. Rocha, M. Evangelisti, E. K. Brechin and S. P. Perlepes, *Dalton Trans.*, 2008, 3153.

22 D. S. Boltin, N. A. Bokach and V. Yu. Kukushkin, *Coord. Chem. Rev.*, 2016, **313**, 62.

23 H.-Z. Kou, G.-Y. An, C.-M. Ji, B.-W. Wang and A.-L. Cui, *Dalton Trans.*, 2010, 9604.

24 C.-M. Ji, H.-J. Yang, C.-C. Zhao, V. Tangoulis, A.-L. Cui and H.-Z. Kou, *Cryst. Growth Des.*, 2009, **9**, 4607.

25 G.-Y. An, H.-B. Wang, A.-L. Cui and H.-Z. Kou, *New J. Chem.*, 2014, **38**, 5037.

26 (*a*) L. Alcazar, M. Font-Bardia and A. Escuer, *Eur. J. Inorg. Chem.*, 2015, 1326; (*b*) J. Jankolovits, C. M. Andolina, J. W. Kampf, K. N. Raymond and V. L. Pecoraro, *Angew. Chem., Int. Ed.*, 2011, **50**, 9660.

27 E. Bernasek, *J. Org. Chem.*, 1957, **22**, 1263.

28 T. Kottke and D. Stalke, *J. Appl. Crystallogr.*, 1993, **26**, 615.

29 APEX2, *Data Collection Software Version 2.1-RC13*, Bruker AXS, Delft, The Netherlands, 2006.

30 Cryopad, *Remote monitoring and control, Version 1.451*, Oxford Cryosystems, Oxford, United Kingdom, 2006.

31 SAINT+, *Data Integration Engine v. 7.23a ©*, Bruker AXS, Madison, Wisconsin, USA, 1997–2005.

32 G. M. Sheldrick, *SADABS v.2.01, Bruker/Siemens Area Detector Absorption Correction Program*, Bruker AXS, Madison, Wisconsin, USA, 1998.

33 G. M. Sheldrick, *SHELXS-97, Program for Crystal Structure Solution*, University of Göttingen, 1997.

34 G. M. Sheldrick, *SHELXL-97, Program for Crystal Structure Refinement*, University of Göttingen, 1997.

35 A. L. Spek, *Acta Crystallogr., Sect. A: Fundam. Crystallogr.*, 1990, **46**, C34; A. L. Spek, *J. Appl. Crystallogr.*, 2003, **36**, 7.

36 P. Van der Sluis and A. L. Spek, *Acta Crystallogr., Sect. A: Fundam. Crystallogr.*, 1990, **46**, 194.

37 C. Papatriantafyllopoulou, C. P. Raptopoulou, A. Terzis, E. Manessi-Zoupa and S. P. Perlepes, *Z. Naturforsch., B: Chem. Sci.*, 2006, **61**, 37.

38 J. Lopez-Carriga, G. T. Badcock and J. F. Harrison, *J. Am. Chem. Soc.*, 1986, **108**, 7241.

39 A. B. P. Lever and A. Mantovani, *Inorg. Chem.*, 1971, **10**, 817.

40 (*a*) F.-R. Dai, D. C. Becht and Z. Wang, *Chem. Commun.*, 2014, 5385; (*b*) B. Biswas, S. Khanra, T. Weyhermuller and P. Chaudhuri, *Chem. Commun.*, 2007, 1059; (*c*) K. V. Shuvaev, S. S. Tandon, L. N. Dawe and L. K. Thompson, *Chem. Commun.*, 2010, 4755; (*d*) H. Jiang, T. Sheng, S. Bai, S. Hu, X. Wang, R. Fu, P. Yu and X. Wu, *Inorg. Chem.*, 2013, **52**, 12305; (*e*) K. Su, F. Jiang, J. Qian, Y. Gai, M. Wu, S. M. Bawaked, M. Mokhtar, S. A. AL-Thabaiti and M. Hong, *Cryst. Growth Des.*, 2014, **14**, 3116.

41 W. H. Press, S. A. Teukolsky, W. T. Vetterling and B. P. Flannery, *Numerical Recipes in C: The Art of Scientific Computing*, Cambridge University Press, Cambridge, 2nd edn, 1992.

42 G.-Y. An, C.-M. Ji, A.-L. Cui and H.-Z. Kou, *Inorg. Chem.*, 2011, **50**, 1079.

43 (*a*) M. Evangelisti, F. Luis, L. J. De Jongh and M. Affronte, *J. Mater. Chem.*, 2006, **16**, 2534; (*b*) M. Evangelisti, Molecular Magnets, NanoScience and Technology, in *Molecule-based Magnetic Coolers: Measurement, Design and Application*, ed. J. Bartolomé, F. Luis and J. F. Fernandez, Springer-Verlag, Berlin, Heidelberg, 2014, pp. 365–387.